molecular pharmaceutics

ARTICLE

pubs.acs.org/molecularpharmaceutics

HSA Coated Iron Oxide Nanoparticles as Drug Delivery Vehicles for Cancer Therapy

Qimeng Quan,[†,‡,§] Jin Xie,[‡,§] Haokao Gao,[‡] Min Yang,[‡] Fan Zhang,[‡] Gang Liu,[‡] Xin Lin,[‡] Andrew Wang,[∥] Henry S. Eden,[¶] Seulki Lee,[‡] Guixiang Zhang,[*,†] and Xiaoyuan Chen[*,‡]

[†]Department of Radiology, Shanghai First People's Hospital, Shanghai Jiaotong University, Shanghai 200080, China

[‡]Laboratory of Molecular Imaging and Nanomedicine (LOMIN), National Institute of Biomedical Imaging and Bioengineering (NIBIB), National Institutes of Health (NIH), Bethesda, Maryland 20892, United States

[∥]Ocean NanoTech, 2143 Worth Lane, Springdale, Arkansas 72764, United States

[¶]Intramural Research Program, National Institute of Biomedical Imaging and Bioengineering (NIBIB), National Institutes of Health (NIH), Bethesda, Maryland 20892, United States

Supporting Information

ABSTRACT: An ongoing effort in the field of nanomedicine is to develop nanoplatforms with both imaging and therapeutic functions, the "nanotheranostics". We have previously developed a human serum albumin (HSA) coated iron oxide nanoparticle (HINP) formula and used multiple imaging modalities to validate its tumor targeting attributes. In the current study, we sought to impart doxorubicin (Dox) onto the HINPs and to assess the potential of the conjugates as theranostic agents. In a typical preparation, we found that about 0.5 mg of Dox and 1 mg of iron oxide nanoparticles (IONPs, Fe content) could be loaded into 10 mg of HSA matrices. The resulting D-HINPs (Dox loaded HINPs) have a hydrodynamic size of 50 nm and are able to release Dox in a sustained fashion. More impressively, the HINPs can assist the translocation of Dox across the cell membrane and even its accumulation in the nucleus. *In vivo*, D-HINPs retained a tumor targeting capability of HINPs, as manifested by both *in vivo* MRI and *ex vivo* immunostaining results. In a follow-up therapeutic study on a 4T1 murine breast cancer xenograft model, D-HINPs showed a striking tumor suppression effect that was comparable to that of Doxil and greatly outperformed free Dox. Such a strategy can be readily extended to load other types of small molecules, making HINP a promising theranostic nanoplatform.

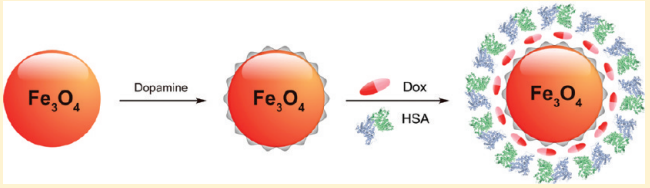

KEYWORDS: iron oxide nanoparticle, theranostic nanomedicine, magnetic resonance imaging, doxorubicin, drug delivery, breast cancer

INTRODUCTION

Many efforts have been witnessed in integrating imaging and therapeutic functionalities into a nanoscale component.[1−4] These efforts are valuable components of the emerging trend toward personalized medicine, which emphasizes tailoring treatments to the biology of individual patients to optimize outcomes. Such a close coupling of imaging and treatment within a theranostic agent and, more importantly, the data about the evolving course of an illness that these agents provide can facilitate informed decisions about modifications to treatment.[5]

Iron oxide nanoparticles (IONPs), being nontoxic, biodegradable and inexpensive, have been previously studied as candidate building blocks for such a purpose.[6,7] However, in most of the investigations, the loading of therapeutics was achieved through covalent binding.[1] This limited the generality of the strategy, since many therapeutics, especially those that are small-molecule based, either are hard to conjugate or may lose their power in a conjugated form. Efforts have been made to prepare porous IONPs that can absorb drug molecules into their cavities.[8,9] Success, however, has been achieved mostly at the *in vitro* level. Alternatively, drug molecules and IONPs can be coloaded into matrices made of liposomes, micelles and polymers.[10−12] For instance, the Jon group loaded IONPs and doxorubicin (Dox) into an anti-biofouling polymer and used the conjugates for the treatment of Lewis lung carcinoma (LLC).[13] Erten et al. developed dextran-core-based stealth liposomal nanoparticles and loaded both IONPs and Dox onto them for imaging and therapy.[14] Meng et al. demonstrated that size reduction and surface functionalization of mesoporous silica nanoparticles (MSNP) with a copolymer enhances the passive delivery of Dox.[15]

In contrast, using proteins as drug carriers has attracted increasing interest, marked by the success of Abraxane as the first FDA approved nanoparticulate drug formula. Essentially a noncovalent complex of HSA and paclitaxel, Abraxane has been proven to have better pharmacokinetics than paclitaxel alone and to be superior to the latter for tumor therapeutics.[16,17] Such success inspired our previous efforts at making HSA-coated IONP (HINPs).[18] We developed a dopamine-plus-HSA method

Received: January 5, 2011
Accepted: August 14, 2011
Revised: August 10, 2011
Published: August 14, 2011

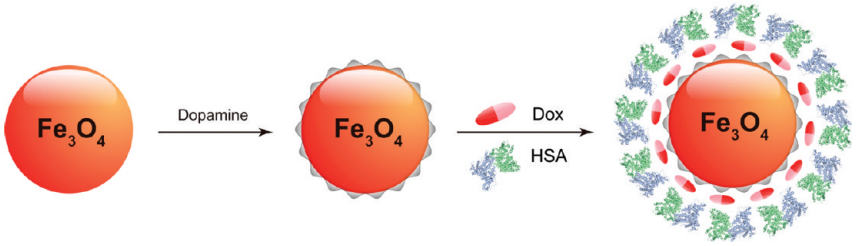

Figure 1. Schematic illustration of the formation of D-HINPs. The as-synthesized IONPs were first surface modified with dopamine to be rendered partially hydrophilic. The resulting dopamine nanoparticles were added, along with Dox, into HSA matrices to form D-HINPs.

to convert oleate coated IONPs to a water-soluble form. We then coupled the resultant particles with radioisotopes (^{64}Cu) and dye molecules (Cy5.5) and studied their distribution in a xenograft tumor model. We found good tumor targeting from PET, NIRF and MR imaging. The current study is an extension of the previous work. We hypothesize that the good ligand binding feature of HSA[3,19,20] will allow further loading of small molecule therapeutics, in this case doxorubicin (Dox), onto the HINPs. The resulting Dox-loaded HINPs (D-HINPs) should have both imaging and therapeutic properties and, more importantly, may improve the therapeutic efficacy of Dox by conferring the tumor targeting properties of HINPs.

MATERIALS AND METHODS

Preparation of D-HINPs. Oleate coated IONPs with a diameter of 15 nm were obtained from Ocean NanoTech (Springdale, AR). For surface modification, about 5 mg of oleate coated nanoparticles were dispersed in 5 mL of chloroform. Then, 20 mg of dopamine in 2 mL of dimethyl sulfoxide (DMSO) was added to the solution. The mixture was stirred to form a homogeneous solution and heated to 70 °C for 1 h. After cooling down to room temperature, the particles were collected via centrifugation, blown dry under nitrogen flow, and redispersed in DMSO with the aid of sonication. In parallel, Dox powder (Sigma-Aldrich) was dissolved in DMSO at a concentration of 16 mg/mL. In a typical preparation, we mixed dopamine coated IONPs (5 mg of Fe/mL in DMSO) and Dox solution, at a volume ratio of 1:1, for 10 min. We then added the solution (in DMSO) dropwise to HSA solution in water (12 mg/mL, 1:7 v/v ratio) with sonication to obtain a homogeneous solution (Figure 1). The particles were collected by centrifugation and were redispersed in PBS buffer solution. For Dox content analysis, a small portion of the product was added to a diluted HCl solution (pH = 5) and incubated for 10 min. The solution was then subjected to fluorescence analysis on a microplate reader (Synergy 2 multimode microplate reader, BioTek). The readout at 590 nm was recorded and compared with a standard curve to determine the concentration. The iron content was analyzed by following a previously published protocol.[21] In brief, a portion of the product was degraded in 50 μL of concentrated HCl, and the solution was then diluted to 1 mL with water. To 12.5 μL of the aliquot, 500 μL of ammonium acetate−acetic acid buffer was added (0.5 M, pH = 3.0), followed by the addition of 25 μL of 10% hydroxylamine hydrochloride to reduce Fe(III) to Fe(II). Finally, 125 μL of 0.3% 1,10-phenanthroline (Sigma-Aldrich) was added to the above solution, and the mixture was incubated at room temperature for 15 min. The absorbance at 511 nm was measured and was compared with a standard curve to calculate the Fe concentration. Freshly made D-HINPs were used in all the studies.

Drug Release Study. To study the drug release, we incubated D-HINPs in PBS (pH 7.4) at 37 °C in a Float-A-Lyzer dialysis tube (molecular weight cutoff 10,000 Da, Pierce) and immersed the tube into 10 mL of PBS in a 15 mL centrifuge tube. At selected time points, 2 mL of the exterior solution was taken out and replaced with fresh PBS. The Dox content was quantified with a microplate reader by comparing with a standard curve.

Cell Culture. The 4T1 murine breast cancer cell line was purchased from the American Type Culture Collection (ATCC) and was cultured in RPMI-1640 medium (FBS, Invitrogen) supplemented with fetal bovine serum (10%, volume percentage) and 1% antibiotics (penicillin, 100 units/mL plus streptomycin) at 37 °C in a humidified incubator containing 5% CO_2.

Cell Toxicity Test. The toxicity of D-HINPs was investigated with 4T1 murine breast cancer cells using 3-(4,5-dimethylthiazol-2-yl)-2,5-diphenyltetrazolium bromide (MTT) assay. In brief, 4T1 cells were seeded, at a density of 5×10^3 cells per well, onto 96-well plates. The assays started 24 h later by incubating the cells with PBS, HINPs, D-HINPs and Dox alone. D-HINPs and Dox were added at the same Dox doses to reach final concentrations of 7.67, 2.56, 0.85, 0.28, 0.095, and 0.032 μg of Dox/mL. The IONPs were added at the same Fe concentrations as in the D-HINP group. After being cultured for 12 and 24 h, the supernatant was discarded by aspiration and each well was washed twice. The cells were then incubated with 200 μL of MTT (0.5 mg/mL) for 4 h at rt, and at the end of the incubation, the supernatant was discarded. Subsequently, 200 μL of DMSO was added into each well and the plates were gently shaken for 5 min. The optical density value at 570 nm was measured by a microreader. Each group was performed three times in quintuplicate.

Cell Internalization of Dox and D-HINPs. *In vitro* studies were performed to elucidate the role of nanoparticles in Dox internaction and intracellular distribution. 4T1 cells were seeded in 8-well Lab-Tek II chamber slides (Thermo Fisher Scientific) at a density of 2×10^4 cells per well and allowed to attach overnight. To facilitate the tracking of the HINP vehicles, we used Cy5.5 labeled HSA for the preparation of D-HINPs. The cells were incubated with free Dox and Cy5.5 labeled D-HINPs (both at 6 μg Dox/mL) at 37 °C in the dark for different time periods (5 min, 30 min and 1 h). After incubation, the slides were washed with PBS and fixed in ice-cold ethanol at −20 °C for 20 min. Subsequently, the slides were washed with PBS and sealed with cover-glasses using mounting medium containing 4′,6-diamidino-2-phenylindole (DAPI). The images were taken on an epifluorescence microscope (Olympus, X81).

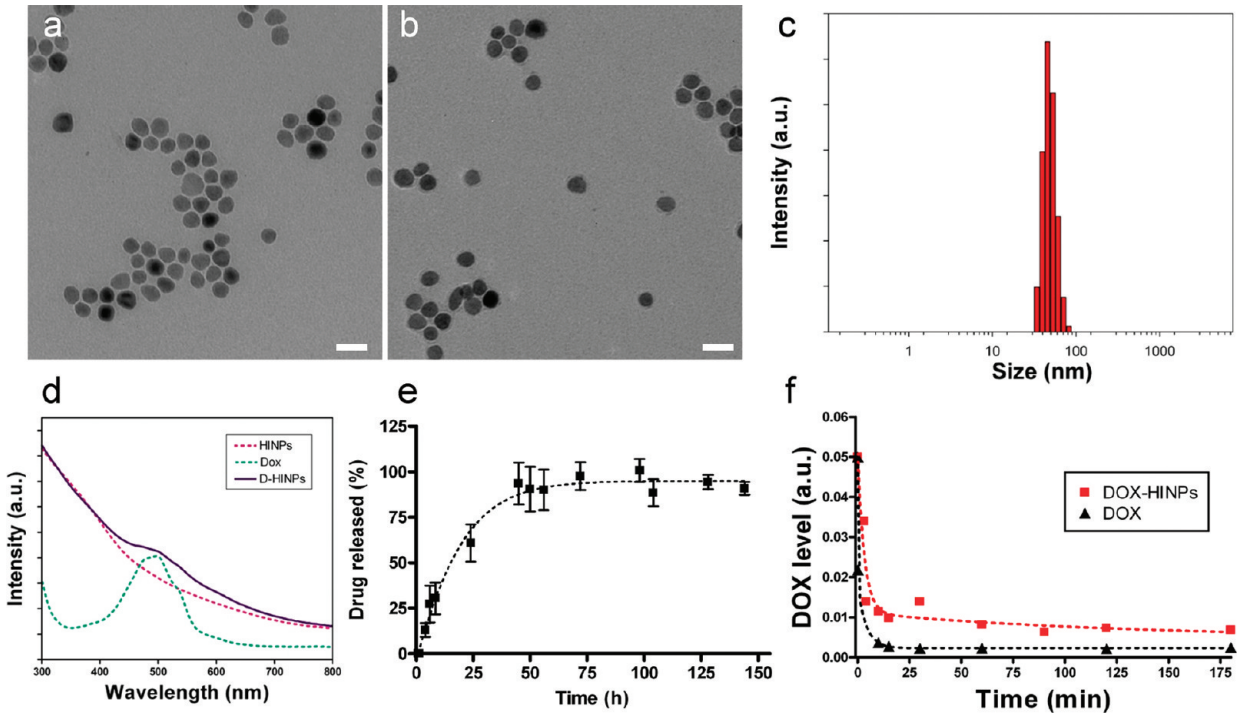

Figure 2. TEM images of (a) oleate-IONPs in hexane and (b) D-HINPs in water. (c) Hydrodynamic size measurement of D-HINPs with dynamic light scattering (DLS). (d) The UV−vis analysis of D-HINPs. (e) Drug release studies performed in PBS at 37 °C. (f) The assessment of circulation half-lives. Simulation was performed with GraphPad using two phase exponential decay.

Determination of Circulation Half-Lives. To determine the circulation half-lives of Dox and D-HINPs, the two formulas were injected iv into healthy nude mice at the same Dox scale (5 mg/kg). At selected time points postinjection (1, 3, 5, 10, 15, 30, 45, 60, 90, and 120 min), about 2−10 μL of blood was collected from the tail vein and dissolved in heparin solution (1,000 U/mL in PBS). The Dox was extracted by acidified isopropanol, and the content was detected on a microplate reader by comparing with a standard curve. The results were plotted as the Dox level against time after injection. The circulation half-lives were evaluated by fitting the results into a two-phase decay model using GraphPad (La Jolla, CA).

Preparation of Animal Model. The 4T1 tumor model was established by subcutaneous injection of 5×10^5 cells in 70 μL of PBS into the right flank of female athymic nude mice (Harlan Laboratories). The imaging started when the tumor volume reached about 500 mm^3. All animal studies were performed in compliance with the principles and procedures outlined in the Guide for the Care and Use of Laboratory Animals[22] and were approved by the Institutional Animal Care and Use Committee of the Clinical Center, National Institutes of Health.

***In Vivo* MR Imaging.** D-HINPs were injected through the tail vein (6 mg of Fe/kg) into the anesthetized mice. Three-dimensional gradient-echo scan (FLASH) images were acquired on a 7.05 T small-animal MR scanner (Bruker Biospin) before injection and 1 h and 4 h postinjection (p.i.). The following parameters were adopted in data acquisition: TR = 200 ms, TE = 4.3 ms, thickness 1.1 mm, FOV 2.8 × 2.56 cm, NEX 12.0, Echo 1/1. For each data set, one slice with comparable locations within the tumor was selected to determine signal intensities. Large necrotic areas were avoided. Signal intensities were measured in defined regions of interest (ROIs) with Image J (National Institutes of Health) for tumor (SI_{tumor}) and noise (SI_{noise}). For SI_{tumor} measurement, ROIs were carefully drawn around the tumors, including the whole tumor where possible. The tumor signal-to-noise ratio (SNR) was defined as $SNR = SI_{tumor}/SI_{noise}$. Relative contrast enhancement was defined as $(SNR_{pre} - SNR_{post})/SNR_{pre} \times 100\%$, where SNR_{pre} was the tumor SNR from the pre-enhanced scan and SI_{post} was the SNR from the postenhanced scan at 1 or 4 h p.i.

***Ex Vivo* Immunostaining.** 4T1 tumor bearing mice were injected intravenously with Dox or D-HINPs (3 mg/kg Dox). The mice were sacrificed 1 and 24 h p.i. The tumor tissues were collected and kept in OCT at −80 °C. The frozen tissue blocks were sectioned into slices of 6−8 μm thickness. The slices were then fixed with cold acetone for 20 min and dried in the air at room temperature in the dark. After being washed with PBS 3 times (5 min each), the slices were mounted with DAPI-containing mounting medium and subjected to imaging with a fluorescence microscope (Olympus, X81).

Biodistribution Studies. 4T1 tumor bearing mice were injected with Dox, D-HINPs at the same Dox dose (5 mg/kg) and were sacrificed at 1, 4, and 24 h p.i. time points (n = 3/group). Tumors and major organs were collected and weighed, and they were then homogenized by nitric acid overnight at room temperature. All the samples were subjected to centrifugation at 14,000 rpm for 10 min to remove the tissue debris. The supernatant was collected, and the Dox content was measured on a microplate reader by comparing with the standard curve. In particular, blood samples were diluted with 20 μL of heparin solution (1,000 U/mL, in PBS) and were treated by following a published protocol.[23] The final Dox concentrations were reported as percentage of injected dose per gram tissue (% ID/g).

Therapeutic Studies. For therapeutic studies, 25 mice were divided into 5 groups (n = 5/group), and were treated with (1)

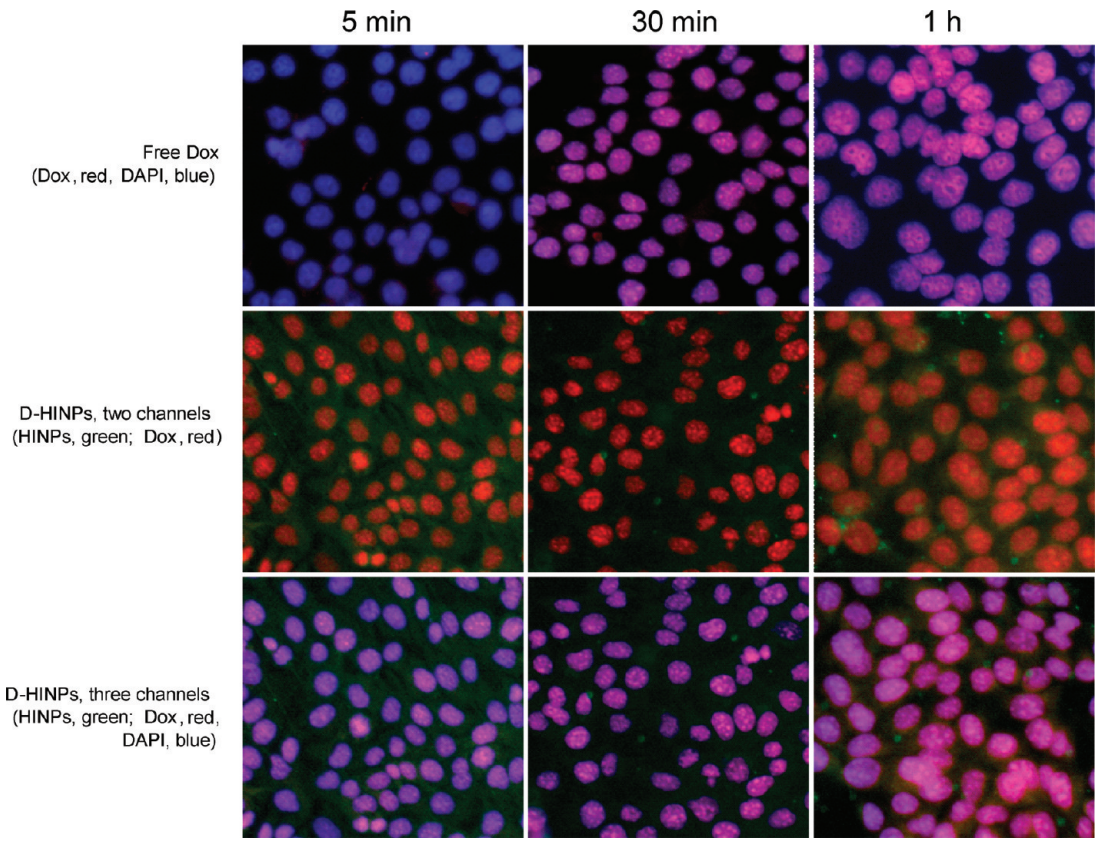

Figure 3. Fluorescence microscopy analysis. 4T1 cells were incubated with free Dox and Cy5.5 labeled D-HINPs at the same Dox concentration (6 μg of Dox/mL). The images were taken at 5, 30, and 60 min after the start of the incubation. Red, Dox; green, Cy5.5; blue; DAPI.

D-HINPs (3 mg of Dox/kg); (2) free Dox (3 mg of Dox/kg); (3) Doxil (3 mg of Dox/kg); (4) HINPs or (5) PBS. For group 4, HINPs were injected at the same Fe concentration as in group 1. The drugs (including controls) were given every other day for a total of 4 doses. The tumor sizes were measured by a digital caliper every other day and calculated by the following equation: volume = (tumor length) $\times$ (tumor width)^2/2. The body weights of tumor mice were recorded every other day.

Statistical Analysis. Quantitative data were expressed as mean $\pm$ SD. Means were compared using Student's *t* test. *P* values of <0.05 were considered statistically significant.

RESULTS

Characterization of D-HINPs. Dox loading was achieved by adding Dox, along with dopamine coated IONPs, into an aqueous solution of HSA (Figure 1). In a typical preparation, we found that 0.5 mg of Dox and 1 mg of IONPs can be loaded into 10 mg of HSA matrices, i.e., in the final formulation, the Dox/Fe/HSA ratio is 1:2:20 (w/w/w) (Figure 2). Such a high loading rate of both nanoparticles and Dox was attributed to the excellent ligand binding capacity of HSA. No morphology change was found for the IONP cores before and after surface modification (Figure 2). The D-HINPs showed good solubility in aqueous solution, and dynamic light scattering (DLS) analysis found an overall size of 50.8 $\pm$ 5.2 nm for the D-HINPs, which is larger than HINPs alone (about 30 nm[18]). The loaded drug can be released in a controlled fashion from the nanoplatform. As shown in Figure 2e, it took a span of 75 h for a complete release of the loaded Dox in PBS.

Cellular Toxicity and Imaging Studies. MTT assays found no inhibitive effects of HINPs against cell growth (Figure S1 in the Supporting Information). As a matter of fact, even slightly increased viability was observed at higher Fe concentrations, which is in accordance with our previous observations and those of others who used different IONP formulas.[24] The D-HINPs, on the other hand, showed concentration dependent inhibitive effects on cell viability, a pattern that is similar to that of Dox alone (Figure S1 in the Supporting Information).

There are two possible pathways that Dox could take to translocate cell membranes. One is that the Dox is released in the intercellular space and penetrates the cell membrane by itself. The other possibility is that the Dox crosses the membrane as a cargo along with HINPs, and is released intracellularly. To elucidate this, we incubated Dox and D-HINPs with 4T1 cells, and monitored the movement of Dox using fluorescence microscopy (Figure 3). In the Dox group, we found that Dox was initially distributed in the cytoplasm (at 5 min), but later concentrated in the nuclei, where it is expected to exert therapeutic power. For D-HINPs, however, such a process was accelerated, as intensive Dox signals were found in the nuclei merely 5 min after the start of incubation. On the other hand, the HINPs were found exclusively in the cytoplasm, which is not surprising considering their size. These observations suggest that HINPs, at least at early time points, played a significant role in transporting Dox. At late time points, however, we saw no obvious difference in cell uptake between the Dox and D-HINP groups.

Pharmacokinetic Studies and MR Imaging. Compared with Dox alone, the D-HINPs showed a much longer circulation

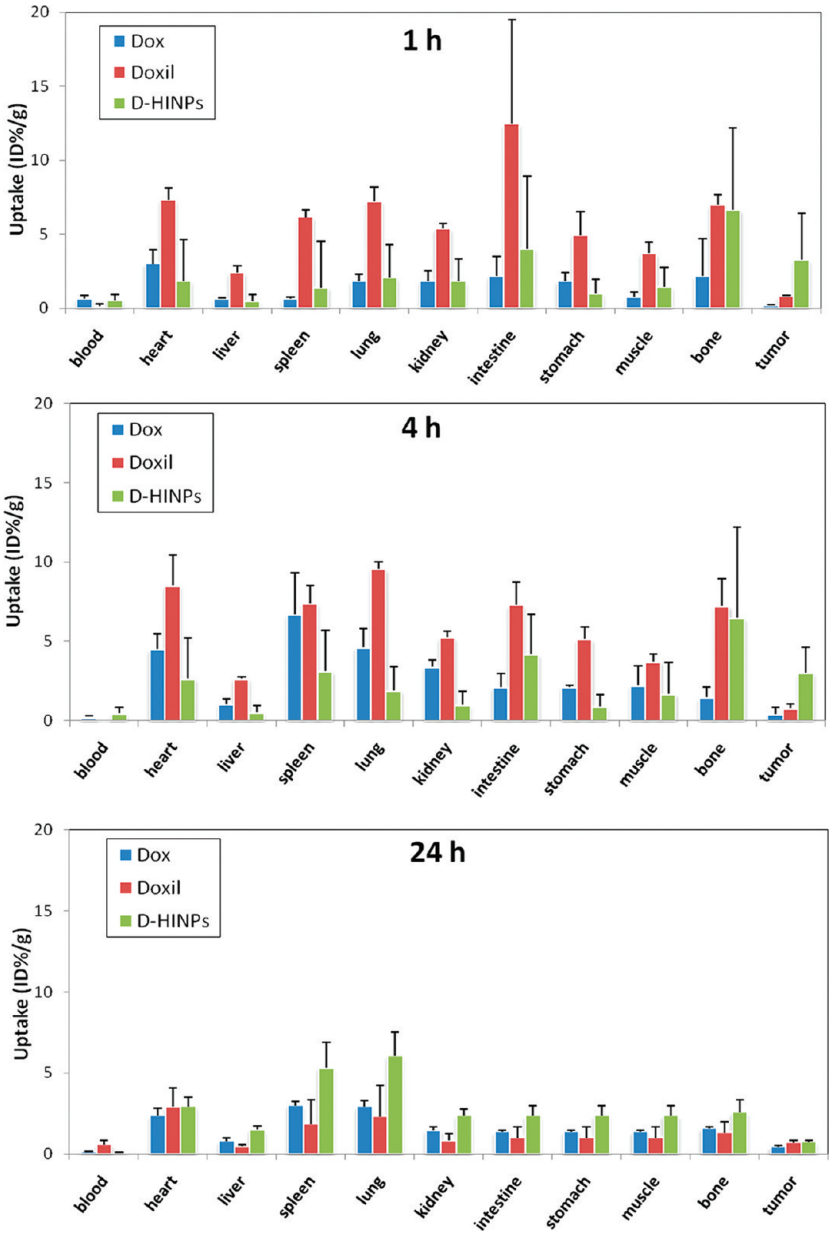

Figure 4. Biodistribution studies. Dox, Doxil and D-HINPs were injected iv at the same dose (5 mg of Dox/kg), and the mice were sacrificed 1, 4, and 24 h after injection for Dox analysis.

half-life (86.9 min vs 2.9 min, two phase exponential decay, Figure 2f). This suggests a significant role for HINP in *in vivo* drug delivery. To further investigate the role of HINP as a vehicle, we injected Dox, D-HINPs, and Doxil (a liposome-based Dox formula that is used in the clinic for the treatment of various cancer types) into 4T1 tumor mice and studied the Dox distribution (Figure 4). The animals were sacrificed, 4, and 24 h after the injection, and the tumors, along with major organs, were collected for Dox extraction and analysis. Tumor uptake of 0.21 ± 0.03 and $0.39 \pm 0.41\%$ ID/g was observed for Dox alone at 1 and 4 h. It was improved in the Doxil case, where tumor uptakes of 0.84 ± 0.05 and $0.78 \pm 0.24\%$ ID/g were observed at 1 and 4 h, respectively. D-HINPs greatly outperformed both formulas, showing tumor uptake of 3.25 ± 3.15 ($P < 0.01$ versus Dox and Doxil treated groups) and 3.03 ± 1.56 ($P < 0.01$ versus Dox and Doxil treated groups), respectively, at 1 and 4 h time points. At the 24 h time point, tumors still showed higher Dox accumulation for D-HINP ($0.75 \pm 0.09\%$ ID/g) and Doxil ($0.69 \pm 0.14\%$ ID/g) than that for free Dox ($0.44 \pm 0.10\%$ ID/g). Such difference in tumor targeting was further confirmed by immunostaining results (Figure S2 in the Supporting Information).

Furthermore, significant hypointensity was found in the tumor area after the probe injection, as tumor/muscle ratio dropped by $26.1 \pm 5.2\%$ and $42.1 \pm 4.3\%$ at 1 and 4 h after the D-HINP injection (Figure 5). Such a correlation between high drug concentration and high hypointensities on the MRI map suggested the role D-HINPs played as a drug delivery vehicle.

Therapeutic Studies. We next moved to therapeutic studies to see whether the good pharmacokinetics of D-HINPs would lead to improved therapeutic outcome. The studies were performed on a 4T1 murine breast cancer model. In brief, Dox,

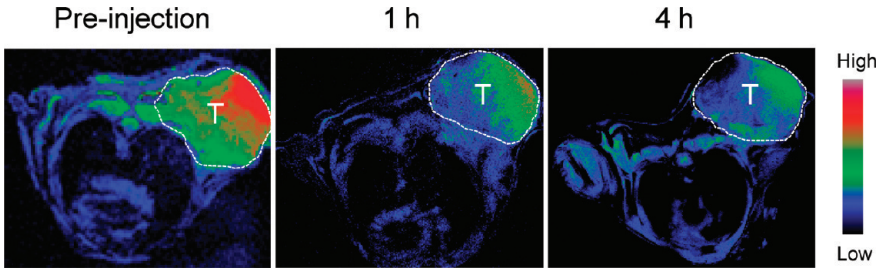

Figure 5. MR images taken before, and 1 and 4 h after the injection of D-HINPs (6 mg of Fe/mL). The contrast enhancement, defined as $(SNR_{pre} - SNR_{post})/SNR_{pre} \times 100\%$, was evaluated to be 26.1 ± 5.2% and 42.1 ± 4.3% at 1 and 4 h p.i. Such a signal decrease was the result of accumulation of HINPs in the tumor area.

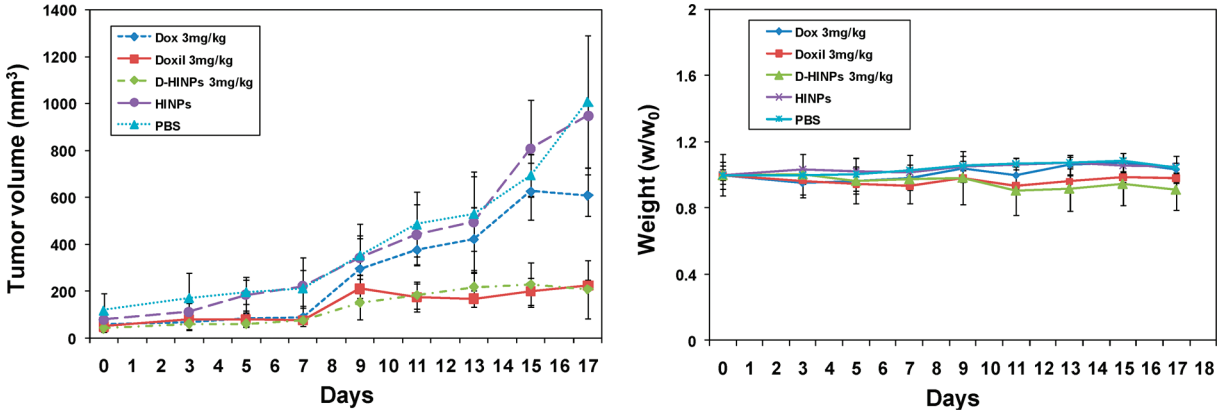

Figure 6. Left: tumor growth curves for treatment with (1) D-HINPs (3 mg of Dox/kg); (2) free Dox (3 mg of Dox/kg); (3) Doxil (3 mg of Dox/kg); (4) HINPs (with same Fe concentration as in 1) and (5) PBS. D-HINPs showed similar therapeutic efficacy to Doxil and greatly outperformed free Dox. Right: change of mouse body weight during treatment (n = 5/group).

D-HINPs and Doxil were injected at a dose of 3 mg of Dox/kg via the tail vein every two days. In control groups, PBS and HINPs (at the same Fe concentration as for the D-HINPs) were injected at the same frequency. The tumor growth was carefully monitored every other day throughout the study. As shown in Figure 6, a steady growth in tumor size was witnessed in the PBS control group. By the end of the treatment course, an average tumor volume of 1010.0 mm^3 was recorded. The group injected with HINPs manifested a tumor growth pattern that was similar to that of the PBS group (948.3 mm^3 on day 17), indicating that the HINPs alone had neither therapeutic nor toxic effects in the studied mice. Compared with the control group, the injection of Dox led to some tumor suppression in the first week (88.5 mm^3 on day 7, compared to that of 212.4 mm^3 for the PBS group and 220.8 mm^3 for the HINPs group) of treatment but gradually lost efficacy. The D-HINPs, on the other hand, showed sustained effects against tumor growth. On day 17, the tumor volume had grown by 395% for the D-HINP group, which was close to the value for Doxil (349%), but superior to Dox alone (979%). A slight weight loss for both Doxil (2.0 ± 0.3%) and D-HINPs (8.9 ± 1.2%) was observed.

DISCUSSION

This study was an extension of our previous work of constructing an HSA-coated iron oxide nanoparticle formula for tumor targeting and imaging. Such a preparation method has the following advantages: first, the core IONPs, made by pyrolysis, can be prepared in kilogram scale with excellent quality control;[25] second, both the inner and outer coating (dopamine and HSA) are biologically safe materials and are available in large quantities at relatively low cost; third, all of the surface modifications can be done at room temperature without the use of chemical conjugation techniques; and last, but not least, the excellent ligand binding capacity of HSA may allow further loading of drug molecules into the nanosystem.

In the current work, we successfully loaded Dox onto such a nanoplatform and studied the therapeutic role of the resulting conjugates. The hydrodynamic size of the resulting D-HINPs was evaluated to be 50.8 nm, which is larger than HINPs alone. Two factors may have contributed to such an increase in nanoparticle size. One is the addition of the Dox filling; the other is the partial aggregation formed through the drug loading and subsequent purification processes. Since larger nanoparticles tend to have much stronger signals under DLS, even a small portion of aggregation can cause a significant shift of the average size value. Nonetheless, the resulting nanoparticles are remarkably smaller than Dox−HSA complex particles (150 to 500 nm[26]). We attributed this to a scaffold role the IONP plays in the nanosystem. As a template of compact size (15 nm), the IONP cores limited the number of HSA that could be adsorbed on their surface and therefore led to nanostructures of a smaller overall size.

In vitro assays found that such HINPs can help Dox to cross the cell membrane and to accumulate in the nucleus. Although the detailed mechanism is unknown at this stage, it can be attributed to the polyamine inner coating layer of the nanostructures, which is positively charged and partially exposed to the

intracellular environment.[24] This feature has been proven in our previous studies as an important factor in facilitating the uptake of HINPs by a number of cell lines.[24] It is possible that the same feature helped the Dox molecule, a relatively hydrophilic compound, to translocate cell membrane via endocytosis. Subsequently in the endosomes/lysosomes, where pH is lower, the interaction between Dox and HSA, presumably hydrogen bonding-based, would be weakened. As a result, the Dox would be released into the cytoplasm and, ultimately, accumulates in the nuclei.

The circulation half-lives of both Dox and D-HINPs showed a two-phase decay pattern, featuring an initial sharp intensity-dropping phase and a second, moderately subsiding phase. The first, distribution phase, indicates a process where Dox distributes among the various tissues. The second, elimination phase, suggests the decline of drug level in all the compartments. It is clear that free Dox is more susceptible to clearance (such as by renal clearance). Dox in D-HINPs, on the other hand, stand much longer in the elimination phase, due to its association with the long circulating HINPs.

Biodistribution studies observed tumor uptakes of 3.25 and 3.03% ID/g for the D-HINPs at 1 and 4 h, which were 15.6 and 7.8 times higher than Dox alone at the same times. Such improved pharmacokinetics is in large part due to the size of D-HINPs. With a size of about 50 nm, D-HINPs are too large to be cleared through the renal route, but, at the same time, are less likely than larger formulas, such as Doxil, to provoke reticuloendothelial system (RES) scavenging. Indeed, we found liver uptake of Dox at 2.41 ± 0.44 and 2.66 ± 0.12% ID/g for the Doxil group at 1 and 4 h, respectively, which is much higher than the uptake of D-HINPs at the same time points (0.45 ± 0.47 and 0.53 ± 0.41% ID/g at 1 and 4 h p.i.). In addition to the size, the HSA coating may have also played a positive role in tumor targeting. As in the case of Abraxane, the HSA sheath may interact with glycoprotein (gp60) receptor (albondin) and SPARC (secreted protein, acidic, rich in cysteine) and, as a result, lead to improved extravasation and tumor accumulation.[18,27]

It is worth pointing out that there is a discrepancy in tumor uptake between the MRI observation and that from the biodistribution study by analyzing Dox content. For Dox analysis, we found little difference in tumor uptake between the 1 and 4 h time points. For MRI, however, we observed an appreciable signal drop, indicating an increased accumulation of particles. The reason, we believe, is attributable to the fact that a portion of nanoparticles did not extravasate but stayed within the vessel lumen. For those D-HINPs that stayed in the vessels, they contributed, in a relatively persistent manner, to the regional hypointensities. Meanwhile, the Dox was gradually released from the HINP platforms. Compared with HINPs, Dox is much easier to be drained or washed away, which offsets the increased particle accumulation.

Such improved pharmacokinetics of D-HINPs explains their much improved therapeutic effects compared to free Dox. At the end of the treatment, the tumor volume had increased by 979% for the Dox group. In the D-HINP group, on the other hand, the growth was significantly less (395%), an effect which was comparable to the clinically used formula Doxil (349%). Despite the fact that D-HINPs showed much higher tumor accumulation of Dox than Doxil at early time points, such difference was diminished at late time points. The exact reason for this is unknown; however, we believe it is related to the nanoparticle constitution and architecture. Despite a more compact overall size, D-HINPs possess a core that is much more rigid (made of iron oxide) than Doxil. In addition, aggregation of D-HINPs could have formed during circulation, especially when a group of D-HINPs were squeezing through narrow vessels and capillaries. Both factors could lead to reduced extravasation rate of D-HINPs. Indeed, *ex vivo* studies on tumor tissues taken 24 p.i. showed similar levels of intracellular tumor accumulation of Dox for both D-HINPs and Doxil, which explains the comparable treatment efficacy of D-HINP and Doxil in the 4T1 tumor model.

The similar therapeutic efficacy of D-HNIP to Doxil, however, should not discourage more investigations with the D-HINP formula. As it is well-known, the most serious adverse effect of Dox treatment is its damage to the heart.[28] This can be life-threatening and, oftentimes, a dose limiting factor. In the current study, however, we found that the Dox accumulation rate in the heart was significantly reduced in the D-HINP group at earlier time points than both Doxil and free Dox. This is a notion worth further exploits, and the related investigations are currently underway.

CONCLUSIONS

In summary, we have successfully transformed HINP into a tumor targeting nanoplatform that possesses both imaging and therapeutic functions. This was achieved by encapsulating Dox, together with dopamine coated IONPs, into HSA matrices. Both *in vivo* imaging and *ex vivo* biodistribution studies confirmed the tumor targeting feature of the resulting D-HINPs. In a therapeutic study on a xenograft 4T1 murine breast cancer model, D-HINPs showed a suppression effect that was comparable to Doxil and significantly better than free Dox. The preparation can be easily scaled up, and the same technique can be readily applied to load other small-molecule-based therapeutics.

ASSOCIATED CONTENT

Supporting Information. DLS measurement, *ex vivo* immunostaining and MTT assay results. This material is available free of charge via the Internet at http://pubs.acs.org.

AUTHOR INFORMATION

Corresponding Authors

*G.Z.: e-mail, guixiangzhang@sina.com. X.C.: National Institutes of Health, 31 Center Dr., Building 31, 1C22, Bethesda, Maryland 20892; e-mail, shawn.chen@nih.gov; tel, 301-451-4246; fax, 301-435-4699.

Author Contributions

§These authors contributed equally to this work.

ACKNOWLEDGMENT

This work was supported by the Intramural Research Program (IRP) of the National Institute of Biomedical Imaging and Bioengineering (NIBIB), NIH and the International Cooperative Program of National Science Foundation of China (NSFC) (81028009). Q.Q. is enrolled in the NIH Graduate Partnerships Program (GPP) and partially supported by the China Scholarship Council (CSC). J.X. is partially supported by an NIH Pathway to Independence Grant (K99/R00). S.L. acknowledges a National Research Council Research Associateship Award

funded by the National Institute of Standards and Technology (NIST) and the IRP of NIBIB, NIH.

REFERENCES

(1) Xie, J.; Lee, S.; Chen, X. Nanoparticle-based theranostic agents. *Adv. Drug Delivery Rev.* **2010**, *62*, 1064–79.

(2) Lukianova-Hleb, E. Y.; Oginsky, A. O.; Samaniego, A. P.; Shenefelt, D. L.; Wagner, D. S.; Hafner, J. H.; Farach-Carson, M. C.; Lapotko, D. O. Tunable plasmonic nanoprobes for theranostics of prostate cancer. *Theranostics* **2011**, *1*, 3–17.

(3) Jeong, H.; Huh, M.; Lee, S. J.; Koo, H.; Kwon, I. C.; Jeong, S. Y.; Kim, K. Photosensitizer-conjugated human serum albumin nanoparticles for effective photodynamic therapy. *Theranostics* **2011**, *1*, 230–9.

(4) Huang, P.; Xu, C.; Lin, J.; Wang, C.; Wang, X.; Zhang, C.; Zhou, X.; Guo, S.; Cui, D. Folic Acid-conjugated Graphene Oxide loaded with Photosensitizers for Targeting Photodynamic Therapy. *Theranostics* **2011**, *1*, 240–50.

(5) Xie, J.; Liu, G.; Eden, H. S.; Ai, H.; Chen, X. Surface-engineered magnetic nanoparticle platforms for cancer imaging and therapy. *Acc. Chem. Res.* **2011**, DOI: 10.1021/ar200044b.

(6) Xie, J.; Huang, J.; Li, X.; Sun, S.; Chen, X. Iron oxide nanoparticle platform for biomedical applications. *Curr. Med. Chem.* **2009**, *16*, 1278–94.

(7) Corot, C.; Robert, P.; Idee, J. M.; Port, M. Recent advances in iron oxide nanocrystal technology for medical imaging. *Adv. Drug Delivery Rev.* **2006**, *58*, 1471–504.

(8) Cheng, K.; Peng, S.; Xu, C.; Sun, S. Porous hollow Fe_3O_4 nanoparticles for targeted delivery and controlled release of cisplatin. *J. Am. Chem. Soc.* **2009**, *131*, 10637–44.

(9) Piao, Y.; Kim, J.; Bin Na, H.; Kim, D.; Baek, J. S.; Ko, M. K.; Lee, J. H.; Shokouhimehr, M.; Hyeon, T. Wrap-bake-peel process for nanostructural transformation from beta-FeOOH nanorods to biocompatible iron oxide nanocapsules. *Nat. Mater.* **2008**, *7*, 242–247.

(10) Yang, X.; Grailer, J. J.; Rowland, I. J.; Javadi, A.; Hurley, S. A.; Steeber, D. A.; Gong, S. Multifunctional SPIO/DOX-loaded wormlike polymer vesicles for cancer therapy and MR imaging. *Biomaterials* **2010**, *31*, 9065–73.

(11) Guthi, J. S.; Yang, S. G.; Huang, G.; Li, S.; Khemtong, C.; Kessinger, C. W.; Peyton, M.; Minna, J. D.; Brown, K. C.; Gao, J. MRI-visible micellar nanomedicine for targeted drug delivery to lung cancer cells. *Mol. Pharmaceutics* **2010**, *7*, 32–40.

(12) Jain, A. K.; Swarnakar, N. K.; Das, M.; Godugu, C.; Singh, R. P.; Rao, P. R.; Jain, S. Augmented anticancer efficacy of doxorubicin-loaded polymeric nanoparticles after oral administration in a breast cancer induced animal model. *Mol. Pharmaceutics* **2011**, *8*, 1140–51.

(13) Yu, M. K.; Jeong, Y. Y.; Park, J.; Park, S.; Kim, J. W.; Min, J. J.; Kim, K.; Jon, S. Drug-loaded superparamagnetic iron oxide nanoparticles for combined cancer imaging and therapy in vivo. *Angew. Chem., Int. Ed.* **2008**, *47*, 5362–5.

(14) Erten, A.; Wrasidlo, W.; Scadeng, M.; Esener, S.; Hoffman, R.; Bouvet, M.; Makale, M. Magnetic resonance and fluorescence imaging of doxorubicin-loaded nanoparticles using a novel in vivo model. *Nanomedicine* **2010**, *6*, 797–807.

(15) Meng, H.; Xue, M.; Xia, T.; Ji, Z.; Tarn, D. Y.; Zink, J. I.; Nel, A. E. Use of size and a copolymer design feature to improve the biodistribution and the enhanced permeability and retention effect of Doxorubicin-loaded mesoporous silica nanoparticles in a murine xenograft tumor model. *ACS Nano* **2010**, *5*, 4131–44.

(16) Conlin, A. K.; Seidman, A. D.; Bach, A.; Lake, D.; Dickler, M.; D'Andrea, G.; Traina, T.; Danso, M.; Brufsky, A. M.; Saleh, M.; Clawson, A.; Hudis, C. A. Phase II trial of weekly nanoparticle albumin-bound paclitaxel with carboplatin and trastuzumab as first-line therapy for women with HER2-overexpressing metastatic breast cancer. *Clin. Breast Cancer* **2010**, *10*, 281–7.

(17) Iglesias, J. nab-Paclitaxel (Abraxane(R)): an albumin-bound cytotoxic exploiting natural delivery mechanisms into tumors. *Breast Cancer Res.* **2009**, *11* (Suppl. 1), S21.

(18) Xie, J.; Chen, K.; Huang, J.; Lee, S.; Wang, J.; Gao, J.; Li, X.; Chen, X. PET/NIRF/MRI triple functional iron oxide nanoparticles. *Biomaterials* **2010**, *31*, 3016–22.

(19) Gradishar, W. J. Albumin-bound paclitaxel: a next-generation taxane. *Expert Opin. Pharmacother.* **2006**, *7*, 1041–53.

(20) Paal, K.; Muller, J.; Hegedus, L. High affinity binding of paclitaxel to human serum albumin. *Eur. J. Biochem.* **2001**, *268*, 2187–91.

(21) Jain, T. K.; Reddy, M. K.; Morales, M. A.; Leslie-Pelecky, D. L.; Labhasetwar, V. Biodistribution, clearance, and biocompatibility of iron oxide magnetic nanoparticles in rats. *Mol. Pharmaceutics* **2008**, *5*, 316–27.

(22) *Guide for the Care and Use of Laboratory Animals*; National Academy Press: Washington, DC, 1996.

(23) MacKay, J. A.; Chen, M.; McDaniel, J. R.; Liu, W.; Simnick, A. J.; Chilkoti, A. Self-assembling chimeric polypeptide-doxorubicin conjugate nanoparticles that abolish tumours after a single injection. *Nat. Mater.* **2009**, *8*, 993–9.

(24) Xie, J.; Wang, J.; Niu, G.; Huang, J.; Chen, K.; Li, X.; Chen, X. Human serum albumin coated iron oxide nanoparticles for efficient cell labeling. *Chem. Commun. (Cambridge)* **2010**, *46*, 433–5.

(25) Park, J.; An, K. J.; Hwang, Y. S.; Park, J. G.; Noh, H. J.; Kim, J. Y.; Park, J. H.; Hwang, N. M.; Hyeon, T. Ultra-large-scale syntheses of monodisperse nanocrystals. *Nat. Mater.* **2004**, *3*, 891–895.

(26) Dreis, S.; Rothweiler, F.; Michaelis, M.; Cinatl, J., Jr.; Kreuter, J.; Langer, K. Preparation, characterisation and maintenance of drug efficacy of doxorubicin-loaded human serum albumin (HSA) nanoparticles. *Int. J. Pharm.* **2007**, *341*, 207–14.

(27) Chen, K.; Xie, J.; Chen, X. RGD-human serum albumin conjugates as efficient tumor targeting probes. *Mol. Imaging* **2009**, *8*, 65–73.

(28) Cai, C.; Lothstein, L.; Morrison, R. R.; Hofmann, P. A. Protection from doxorubicin-induced cardiomyopathy using the modified anthracycline N-benzyladriamycin-14-valerate (AD 198). *J. Pharmacol. Exp. Ther.* **2010**, *335*, 223–30.